
Whitening and Coloring transform for GANs

Aliaksandr Siarohin
DISI, University of Trento, Italy
aliaksadr.siarohin@unitn.it

Enver Sangineto
DISI, University of Trento, Italy
enver.sangineto@unitn.it

Nicu Sebe
DISI, University of Trento, Italy
niculae.sebe@unitn.it

Abstract

Batch Normalization (BN) is a common technique used both in discriminative and generative networks in order to speed-up training. On the other hand, the learnable parameters of BN are commonly used in conditional Generative Adversarial Networks for representing class-specific information using conditional Batch Normalization (cBN). In this paper we propose to generalize both BN and cBN using a Whitening and Coloring based batch normalization. We apply our method to conditional and unconditional image generation tasks and we show that replacing the BN feature *standardization* and scaling with our feature whitening and coloring improves the final qualitative results and the training speed. We test our approach on different datasets and we show a consistent improvement orthogonal to different GAN frameworks. Our CIFAR-10 supervised results are higher than all previous works on this dataset.

1 Introduction

Generative Adversarial Networks (GANs) [1] have drawn much attention in the last years due to their proven ability to generate sufficiently realistic short videos [2] or still images [3], possibly *conditioned* on some input information such as: a class label [4], an image [5], a textual description [6] or structured data [7, 8]. Generally speaking, GAN training is based on an adversarial game between two networks: a generator G , whose goal is to generate data (e.g., images) and a discriminator D , whose task is to discriminate between real data and “fake” data generated by G . When the generation process depends on some input data, the framework is commonly called conditional GAN (cGAN).

In this paper we deal with both conditional and unconditional GANs and we propose to replace Batch Normalization [9] (BN) with a *Whitening and Coloring* transform [10] in order to speed-up training and improve GAN results. BN, proposed in [9] for discriminative tasks and then adopted in many discriminative and generative networks, extends the common practice of input whitening to the input of *all* the network’s layers. Specifically, given a batch of d -dimensional samples $B = \{\mathbf{x}_1, \dots, \mathbf{x}_m\}$, input to a given network layer, BN transforms each sample $\mathbf{x}_i \in \mathbb{R}^d$ in B using:

$$BN(x_i^k) = \gamma_k \frac{x_i^k - \mu_{B,k}}{\sqrt{\sigma_{B,k}^2 + \epsilon}} + \beta_k, \quad (1)$$

where: k ($1 \leq k \leq d$) indicates the k -th dimension of the data, $\mu_{B,k}$ and $\sigma_{B,k}$ are, respectively, the mean and the standard deviation computed with respect to the k -th dimension of the samples in B and ϵ is a constant used to prevent numerical instability. Finally, γ_k and β_k are *learnable* parameters,

which are introduced in [9] in order to prevent losing the original representation capacity of the network. More in detail, γ_k and β_k are used to guarantee that the BN transform can be inverted, if necessary, in order to represent the identity transform [9]. From Eq. (1) it is clear that the BN transform is performed dimension-wise and, hence, instead of feature whitening, BN only deals with feature *standardization*, thus completely ignoring feature *decorrelation*. This is motivated in [9] by the fact that full whitening of each layer’s input is costly and not easily differentiable. In this paper we propose a differentiable solution whose additional computational overhead is minor with respect to the overall cost of the forward and backward passes. Specifically, we propose a batch normalization which is based on a Whitening and Coloring transform (WC) of each \mathbf{x}_i computed as follows:

$$WC(x_i^k) = \Gamma_k \hat{\mathbf{x}}_i + \beta_k \quad (2)$$

$$\hat{\mathbf{x}}_i = W_B(\mathbf{x}_i - \boldsymbol{\mu}_B) \quad (3)$$

In Eq. (3), the vector $\boldsymbol{\mu}_B$ is the mean of the elements in B (being $\mu_{B,k}$ its k -th component) while the matrix W_B is such that: $W_B^\top W_B = \Sigma_B^{-1}$, where Σ_B is the covariance matrix computed using B . The transform in Eq. (3) performs the full *whitening* of \mathbf{x}_i and the resulting set of vectors $\hat{B} = \{\hat{\mathbf{x}}_1, \dots, \hat{\mathbf{x}}_m\}$ lies in a spherical distribution (i.e., with a covariance matrix equal to the identity matrix). Note that, similarly to $\mu_{B,k}$ and $\sigma_{B,k}$ in Eq. (1), $\boldsymbol{\mu}_B$ and W_B are completely data-dependent, being computed using only B and without any learnable parameter involved. On the other hand, Eq. (2) performs the *coloring* transform [10], which projects the elements in \hat{B} onto a multivariate Gaussian distribution with an arbitrary covariance matrix. This is obtained using the *learnable* parameters Γ_k and β_k . Specifically, Γ_k is a *vector* of parameters which generalizes the scalar parameter γ_k in Eq. (1). The motivation behind the coloring transform is similar to the shift-and-scaling transform performed by means of γ_k and β_k in Eq. (1): using Eq. (2) the whitening transform can potentially be inverted by the network, if that were the optimal thing to do [9]. We empirically show (see Sec. 5.1.1) that whitening without coloring performs poorly.

The second novelty we introduce in this paper is specific for a cGAN framework and concerns exploiting the coloring transform introduced above in order to represent class-specific information. Formally, given a set of class labels $\mathcal{Y} = \{1, \dots, n\}$, we want to generate an image $I = G(\mathbf{z}, y)$, where the generator is input with a noise vector \mathbf{z} and a class label y . For instance, if $y = \text{cat}$, we want a foreground object in I depicting a cat, if $y = \text{dog}$, then I should represent a dog, etc. The categorical conditional information y is commonly represented in G using *conditional batch/instance normalization* (cBN) [11], where a *class-specific* pair of parameters $(\gamma_{k,y}, \beta_{k,y})$ is learned for each class y . In the forward-pass, given y as an additional input to G , only the y -specific scaling-shifting parameters are applied in Eq. (1). In the backward pass, only the parameter pair $(\gamma_{k,y}, \beta_{k,y})$ is updated given y . Analogously, in our proposal (cWC) we use class-specific pairs $(\Gamma_{k,y}, \beta_{k,y})$. The intuitive idea behind the proposed cWC is that $\Gamma_{k,y}$ is more informative than the scalar parameter $\gamma_{k,y}$ in [11] and, thus, it can more accurately represent class-specific information.

Finally, in order to have a set of filters $\{\Gamma_{k,y}\}$ which grows sub-linearly with respect to the number of classes n , we use a restricted dictionary of *class-agnostic* filters together with class-filter soft-assignment weights. The use of a class-independent dictionary of filters, together with a class-agnostic branch in the architecture of our cGAN generators (see Sec. 4) makes it possible to share parameters over all classes and to reduce the final number of weights which need to be learned.

In summary, our contributions are the following:

- We propose a whitening-coloring transform for batch normalization. Even if we tested our proposal using only generative tasks, we believe it can be used also for discriminative tasks.
- In a cGAN framework we propose: (1) A class-specific coloring transform which generalizes cBN [11] and (2) A soft-assignment of classes to filters to reduce the network complexity.
- Using different datasets and basic GAN frameworks, we show that our WC and cWC consistently improve the original framework’s results and training speed.

Our code is publicly available¹.

¹<https://github.com/AliaksandrSiarohin/wc-gan>

2 Related Work

Batch Normalization. BN [9] has been proved to speed-up training in many discriminative and generative works and was extended to cBN [11] for conditional generative tasks. Ba et al. [12] propose Layer Normalization, where normalization is performed using the layer’s activation values of a single sample. Luo [13] proposes to whiten the activation values using a *learnable* whitening matrix. Differently from [13], our whitening matrix only depends on the specific batch of data. Moreover, we show that the coloring step is of a crucial importance to boost the network performance.

Representing conditional information in GANs. cGANs have been widely used to produce images conditioned on some input. For instance, Isola et al. [5] transform a given image in a second image represented in another “channel”. Siarohin et al. [8] extend this framework to deal with structured conditional information (the human body pose). In [6] a textual description of an image is used to condition the image generation. When the conditioning information y is a categorical, unstructured variable, as in the case investigated in this paper, y can be represented in different ways. cBN [11] use y to select class-specific scaling and shifting parameters in G (more details in Sec. 4). Another common approach is to represent y using a one-hot vector, which is concatenated with the input layer of D and G [14, 15] or with the first convolutional layer of D [15]. Miyato et al. [16] split the last layer of D in two branches. The first estimates the class-agnostic probability that the input image is real, while the second represents class-conditional information. This solution is orthogonal to our proposed cWC and we show in Sec. 5.2 that the two approaches can be combined for boosting the results obtained in [16].

3 The Whitening and Coloring transform for Batch Normalization

We start describing the details of our Whitening and Coloring transform in the unconditional case (WC) which is based on Eq. (2)-(3). In all the paper we assume an image domain and convolutional generator/discriminator networks. However, most of the solutions we propose can potentially be applied to non-visual domains and non-convolutional networks.

Let $F \in \mathbb{R}^{h \times w \times d}$ be the tensor representing the activation values of the convolutional feature maps for a given image and layer, with d channels and $h \times w$ spatial locations. Similarly to [9], we consider the d channel activations of each location in the $h \times w$ convolutional grid as a separate instance $\mathbf{x}_i \in \mathbb{R}^d$ in B (also known as *instance* normalization [17]). This is done also to have a larger cardinality batch (B) which alleviates instability issues when computing the batch-related parameters. In fact, a mini-batch of m' images corresponds to $m = |B| = m' \times h \times w$ [9].

For notational convenience, we rewrite below Eq. (2)-(3) using a slightly different notation, where $WC(\mathbf{x}_i) = \text{Coloring}(\hat{\mathbf{x}}_i)$ and $\hat{\mathbf{x}}_i = \text{Whitening}(\mathbf{x}_i)$:

$$\text{Coloring}(\hat{\mathbf{x}}_i) = \Gamma \hat{\mathbf{x}}_i + \beta \tag{4}$$

$$\text{Whitening}(\mathbf{x}_i) = W_B(\mathbf{x}_i - \boldsymbol{\mu}_B). \tag{5}$$

In Eq. (4), Γ is a matrix whose k -th row is the channel-specific filter Γ_k and $\beta = (\beta_1, \dots, \beta_k, \dots, \beta_d)^\top$ (see Sec. 1). In order to compute the whitening matrix W_B in Eq. (5), we first need to compute the batch-dependent covariance matrix Σ_B (Sec. 1). Since this computation may be unstable, we use the Shrinkage estimator [18] which is based on blending the empirical covariance matrix $\hat{\Sigma}_B$ with a regularizing matrix (in our case we use I , the identity matrix):

$$\Sigma_B = (1 - \epsilon)\hat{\Sigma}_B + \epsilon I, \text{ where: } \hat{\Sigma}_B = \frac{1}{m-1} \sum_{i=1}^m (\mathbf{x}_i - \boldsymbol{\mu}_B)(\mathbf{x}_i - \boldsymbol{\mu}_B)^\top, \tag{6}$$

Once Σ_B is computed, we use the Cholesky decomposition [19] in order to compute W_B in Eq. (5) such that $W_B^\top W_B = \Sigma_B^{-1}$. Note that the Cholesky decomposition is unique given Σ_B and that it is differentiable, thus we can back-propagate the gradients through our whitening transform (more details in the appendix C). Many modern platforms for deep-network developing such as TensorFlow [20] include tools for computing the Cholesky decomposition. Moreover, its computational cost is

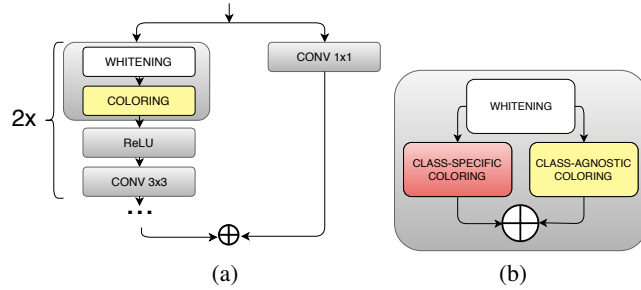


Figure 1: A ResNet block composed of 2 *Whitening-Coloring-ReLU-Conv* sequences (a) and a cWC layer (b).

smaller than other alternatives such as the ZCA whitening [21]. Our preliminary results with the ZCA whitening achieved lower Inception Score values on CIFAR-10. In details, W_B is computed using a lower triangular matrix L and the following steps:

1. We start with $LL^\top = \Sigma_B$, which is equivalent to $L^{-\top}L^{-1} = \Sigma_B^{-1}$.
2. We use the Cholesky decomposition in order to compute L and L^\top from Σ_B .
3. We invert L and we eventually get $W_B = L^{-1}$ which is used in Eq. (5).

On the other hand, the coloring step (Eq. (4)) is a linear operation and can be simply implemented using $1 \times 1 \times d$ convolutional filters Γ_k and the corresponding biases β_k .

WC is plugged before each convolutional layer of our generators. In most of our experiments, we use a ResNet-like architecture [22] for G with 3 blocks [3]. Fig. 1(a) shows a simplified block scheme. We do not use WC nor we introduce any novelty in the discriminators (more details in Sec. 5).

Finally, at inference time, once the network has been trained, W_B and μ_B in Eq. (5) are replaced with the expected W_E and μ_E , computed over the whole population and approximated using the running average as in [9]. In more detail, at each mini-batch training iteration t , we compute an updated version of Σ_E^t and μ_E^t by means of:

$$\Sigma_E^t = (1 - \lambda)\Sigma_E^{t-1} + \lambda\Sigma_B; \quad \mu_E^t = (1 - \lambda)\mu_E^{t-1} + \lambda\mu_B. \quad (7)$$

Once training is finished, we use Σ_E and the 3 steps above described to compute W_E . Note that this operation needs to be done only once, after that W_E and μ_E are fixed and can be used for inference.

3.1 Computational overhead

The computational cost of $Whitening()$ is given by the sum of computing $\hat{\Sigma}_B$ ($O(md^2)$) plus the Cholesky decomposition ($O(2d^3)$), the inversion of L ($O(d^3)$) and the application of Eq. (5) ($O(d^2)$). On the other hand, $Coloring()$ is implemented as a convolutional operation which can be largely sped-up using common GPUs. Overall, with $m \sim d$, WC is $O(d^3)$. Using the ResNet architecture above mentioned with $3 \times 2 + 1 = 7$ WC layers, in our CIFAR-10 experiments (32×32 images), we need 0.82 seconds per iteration on average on a single Titan X. This includes both the forward and the backward pass for 1 generator and 5 discriminator updates [3]. In comparison, the standard BN, with the same architecture, takes on average 0.62 seconds. The ratio WC/BN is 1.32, which is a minor relative overhead. At inference time, since W_E and μ_E are pre-computed, WC is reduced to the application of Eq. (5) and the convolutional operations implementing the coloring transform.

4 Conditional Coloring transform

In a cGAN framework, the conditional information y , input to G , is commonly represented using the *conditional batch/instance normalization* (cBN) [11], where Eq. (1) is replaced with:

$$cBN(x_i^k) = \gamma_{k,y} \frac{x_i^k - \mu_{B,k}}{\sqrt{\sigma_{B,k}^2 + \epsilon}} + \beta_{k,y}. \quad (8)$$

Comparing Eq. (1) with Eq. (8), the only difference lies in the class-specific γ and β parameters, which are used to project each standardized dimension into a class-specific univariate Gaussian distribution. We propose to replace Eq. (8) with our *conditional Whitening and Coloring* transform (cWC): $cWC(\mathbf{x}_i) = CondColoring(\hat{\mathbf{x}}_i)$ and $\hat{\mathbf{x}}_i = Whitening(\mathbf{x}_i)$, where:

$$CondColoring(\hat{\mathbf{x}}_i) = \Gamma_y \hat{\mathbf{x}}_i + \beta_y + \Gamma \hat{\mathbf{x}}_i + \beta. \quad (9)$$

The first term in Eq. (9) is based on class-specific learnable parameters Γ_y and β_y . Analogously to [11], in the forward-pass (both at training and at inference time), conditional information y , input to G , is used to select the correct (Γ_y, β_y) pair to apply. Similarly, during training, gradient information is backpropagated through *only* the corresponding pair used in the forward pass.

The second term in Eq. (9) is based on class-agnostic learnable parameters Γ and β , similarly to the unconditional coloring transform in Eq. (4). The motivation behind the use of this second term is the higher instability of the class-specific (Γ_y, β_y) parameter computation with respect to the corresponding class-agnostic weights. In fact, in a generative task with n classes and a training protocol with batches of m elements, on average only $\frac{m}{n}$ instances in B are associated with label y . Thus, on average, at each training iteration, the parameters (Γ_y, β_y) are updated using an *effective batch* of $\frac{m}{n}$ elements versus a batch of m elements used for all the other class-independent parameters. In Sec. 5.2.1 we empirically show the importance of this second term. Fig. 1(b) shows the two separate network branches corresponding to the two terms in Eq. (9).

4.1 Class-filter soft assignment

When the number of classes n is small and the number of real training images is relatively large, learning a separate pair Γ_y for each y is not a problem. However, with a large n and/or few training data, this may lead to an over-complex generator network which can be hard to be trained. Indeed, the dimensionality of each Γ_y is $d \times d$ and learning nd^2 parameters may be difficult with a large n .

In order to solve this issue, when n is large, we compute Γ_y using a weighted sum over the elements of a class-independent dictionary D . Each row of D contains a flattened version of a Γ matrix. More formally, D is an $s \times d^2$ matrix, with $s \ll n$. The j -th row in D is given by the concatenation of d d -dimensional filters: $D_j = [\Gamma_1^j, \dots, \Gamma_k^j, \dots, \Gamma_d^j]$, $\Gamma_k^j \in \mathbb{R}^d$. D is shared over all the classes. On the other hand, given y as input, Γ_y is computed using:

$$\Gamma_y = \mathbf{y}^\top AD, \quad (10)$$

where \mathbf{y} is a one-hot representation of class y (i.e., a vector of zero elements except one in the y -th component) and it is used to select the y -th row (A_y) of the $n \times s$ association matrix A . During training, given y , only the weights in A_y are updated (i.e., all the other rows $A_{y'}$, with $y' \neq y$ are not used and do not change). However, *all* the elements in D are updated independently of y .

In the rest of the paper, we call (plain) cWC the version in which n different class-specific matrices Γ_y are learned, one per class, and cWC_{sa} the version in which Γ_y is computed using Eq. (10). In all our experiments (Sec. 5.2), we fix $s = \lceil \sqrt{n} \rceil$. The computational cost of both versions is basically the same as WC (Sec. 3.1). In cWC_{sa} , the only additional overhead of the class-specific branch is given by computing $A_y^\top D$, which is $O(sd^2)$.

5 Experiments

We split our experiments in two main scenarios: unconditional and conditional image generation. In each scenario we first compare our approach with the state of the art and then we analyze the impact of each element of our proposal. We use 4 datasets: CIFAR-10, CIFAR-100 [23], STL-10 [24] and Tiny ImageNet². The latter is composed of 64×64 images taken from 200 ImageNet categories (500 images per class). In our evaluation we use the two most common metrics for image generation tasks: Inception Score (IS) [25] (the higher the better) and FID [26] (the lower the better). We use different generator architectures in combination with different discriminator training protocols. The goal is to show that our whitening-coloring transforms can consistently improve the quality of the results with respect to different basic GAN frameworks, training datasets and image generation scenarios. We show examples of generated images in the appendix D. In the appendix B we also show further experiments in which we use the MNIST [27] and the Fashion-MNIST [28] datasets.

In all our experiments, both the WC and the cWC transform, as well as the simplified baselines presented in the ablation studies, are applied before *each* convolutional layer of our generators.

5.1 Unconditional image generation

In the unconditional scenario we use two different training strategies for the *discriminator*: (1) WGAN with Gradient Penalty [3] (*GP*) and (2) GAN with Spectral Normalization [29] (*SN*). Remind that our WC is used only in the generator (Sec. 3). When WC is used in combination with *GP*, we call it *WC GP*, while, in combination with *SN*, we refer to it as *WC SN*. Moreover, we use either ResNet [22, 3] or DCGAN [30] as the basic generator architecture. In order to make the comparison with the corresponding *GP* and *SN* frameworks as fair as possible and to show that the quantitative result improvements are due *only* to our batch normalization approach, we strictly follow the architectural and training protocol details reported in [3, 29]. For instance, in *WC SN + DCGAN* we use the same DCGAN-based discriminator used in *SN + DCGAN* [29], with the same number of feature-map dimension (*d*) in each layer in both the generator and the discriminator, the same learning rate policy, etc. We provide further implementation details in the appendix A.1.

In Tab. 1 we show that WC improves both the IS and the FID values of all the tested frameworks in both the CIFAR-10 and the STL-10 dataset. Specifically, independently of the basic architecture (either ResNet or DCGAN), our WC transform improves the corresponding *SN* results. Similarly, our *WC GP* results are better than the corresponding *GP* values.

Table 1: CIFAR-10 and STL-10 results of different frameworks with and without our WC. The *GP* and *SN* based values (without WC) are taken from the corresponding articles [3, 29]. For completeness, we also report *FID 10k* results following the FID-computation best practice suggested in [26].

Method	CIFAR-10			STL-10		
	IS	FID 5k	FID 10k	IS	FID 5k	FID 10K
GP + ResNet [3]	$7.86 \pm .07$	-	-	-	-	-
WC GP + ResNet (ours)	$8.20 \pm .08$	-	20.4	-	-	-
SN + DCGAN [29]	$7.58 \pm .12$	25.5	-	$8.79 \pm .14$	43.2	-
WC SN + DCGAN (ours)	$7.84 \pm .10$	25.5	23.0	9.45 ± 0.18	40.1	37.9
SN + ResNet [29]	$8.22 \pm .05$	21.7	-	$9.10 \pm .04$	40.1	-
WC SN + ResNet (ours)	$8.66 \pm .11$	20.2	17.2	$9.93 \pm .13$	38.7	36.4

In Tab. 2 (left) we compare *WC SN + ResNet* with other methods on CIFAR-10 and we show that we reach results almost on par with the state of the art on this dataset [31]. Note that the *average* IS values over 10 runs reported in [31] is exactly the same as our *average* IS value: 8.56 (the results reported in the table refer to the best values for each framework). Moreover, the method proposed in [31] is based on a much more sophisticated generator architecture and training protocol.

Finally, in Fig. 2 we plot the IS and the FID values computed at different mini-batch training iterations. These plots empirically show that the proposed batch normalization approach speeds-up the training process. For instance, the IS value of *WC SN + ResNet* after 20k iterations is already higher than the IS value of *SN + ResNet* after 50k iterations.

²<https://tiny-imagenet.herokuapp.com/>

Table 2: CIFAR-10 unsupervised (left) and supervised (right) experiments. Most of the results are taken from [3].

Method	IS	Method	IS
ALI [32]	5.34 ± .05	SteinGAN [38]	6.35
BEGAN [33]	5.62	DCGAN with labels [38]	6.58
DCGAN [30]	6.16 ± .07	Improved GAN [25]	8.09 ± .07
Improved GAN (-L+HA) [25]	6.86 ± .06	AC-GAN [4]	8.25 ± .07
EGAN-Ent-VI [34]	7.07 ± .10	SGAN-no-joint [39]	8.37 ± .08
DFM [35]	7.72 ± .13	WGAN-GP ResNet [3]	8.42 ± .10
WGAN-GP [3]	7.86 ± .07	SGAN [39]	8.59 ± .12
CT-GAN [36]	8.12 ± .12	SNGAN-PROJECTIVE [16]	8.62
SN-GAN [29]	8.22 ± .05	CT-GAN [36]	8.81 ± .13
OT-GAN [37]	8.46 ± .12	AM-GAN [40]	8.91 ± .11
PROGRESSIVE [31]	8.80 ± .13	cWC SN + Proj. Discr. (ours)	9.06 ± .13
WC SN + ResNet (ours)	8.66 ± .11	<i>cWC_{sa}</i> SN + Proj. Discr. (ours)	8.85 ± .10

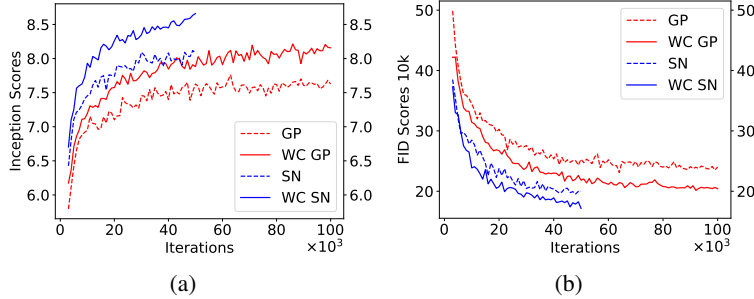


Figure 2: IS (a) and FID 10k (b) values on CIFAR-10 sampled at every 1000 iterations.

5.1.1 Ablation study

We use CIFAR-10 to analyze the influence of each WC element and an SN + ResNet framework [29], omitting 'SN' and 'ResNet' from the names of our baselines for simplicity.

Our initial baseline is *W-only*, in which we use Eq. (5) to project the features in a spherical distribution *without coloring*. In *WC-diag*, after whitening (Eq. (5)), we use Eq. (4) with *diagonal* Γ matrices. This corresponds to learn *scalar* γ - β parameters for a dimension-wise shifting-scaling transform as proposed in [9]. Finally, *WC* is our full-pipeline.

The results reported in Tab. 3 show that feature whitening without coloring performs poorly. We believe this is due to the fact that the activation values, once normalized with *W-only*, have zero mean and thus, on average, half of them are “cut” by the subsequent ReLU nonlinearity. After the feature normalization step, it is crucial for the network to re-project the features in a new (learned) distribution with a sufficient representation capacity. This is done in standard BN [9] using the γ - β parameters. Analogously, in our WC, this role is played by the coloring step. In fact, with a diagonal-matrix based coloring, *WC-diag* improves the results with respect to *W-only*. Moreover, a drastic improvement is obtained by the full-pipeline (*WC*) with respect to *WC-diag*, showing the importance of learning a full covariance matrix in the coloring step.

Table 3: CIFAR-10: Ablation study of WC.

Method	IS	FID 10k
<i>W-only</i>	6.63 ± .07	36.8
<i>WC-diag</i>	7.00 ± .09	34.1
<i>WC</i>	8.66 ± .11	17.2

Table 4: Tiny ImageNet results.

Method	IS	FID 10k
<i>cBN</i>	9.27 ± .14	39.9
<i>cWC</i>	10.43 ± .13	35.7
<i>cWC_{sa}</i>	11.78 ± .25	27.7

5.2 Conditional image generation

In the cGAN scenario, conditional information is represented in the generator as explained in Sec. 4 and using either *cWC* or *cWC_{sa}* (Sec. 4.1).

In Tab. 5 we use different basic discriminator and training-protocol frameworks and we report results with and without our conditional batch normalization approach in the corresponding generator. Similarly to the experiments in Sec. 5.1, in our cWC and cWC_{sa} based GANs we follow the implementation details of the reference frameworks. The only difference with respect to the approaches we compare with (apart our conditional batch normalization) is the number of filters in the discriminator and in the generator (see the Supplementary Material for more details). Tab. 5 shows that both cWC and cWC_{sa} improve the IS and the FID values with respect to the basic frameworks in both the CIFAR-10 and the CIFAR-100 dataset. On CIFAR-10 cWC outperforms cWC_{sa} , probably because, with a small number of classes (n), learning class-specific coloring filters (Γ_y) is relatively easy and more informative than using a class-agnostic dictionary. However, with $n = 200$, as in the case of the Tiny ImageNet dataset, cWC_{sa} obtains significantly better results than cWC (see Tab. 4). In Tab. 4, cBN corresponds to our re-implementation of [16], with a ResNet generator + cBN [11] and an SN + ResNet + *Projection Discriminator* [16]. Note that both cWC and cWC_{sa} significantly improve both the IS and the FID values with respect to cBN on this large and challenging dataset.

Finally, in Tab. 2 (right) we compare cWC and cWC_{sa} with other methods on CIFAR-10, where cWC achieves the best so far published supervised results on this dataset. Note that cWC SN + Proj. Discr. in Tab. 2 (right) and in Tab. 5 indicate exactly the same framework, the only difference being the learning rate policy (see the appendix A.2). In fact, for a fair comparison, in Tab. 5 we strictly adopted the policy used in [16], which has been customized to our approach for the comparison in Tab. 2 (right).

Table 5: CIFAR-10/100: comparing cWC and cWC_{sa} with different basic frameworks.

Method	CIFAR-10			CIFAR-100		
	IS	FID 5k	FID 10k	IS	FID 5k	FID 10K
GP + ACGAN [3]	8.42 ± .10	-	-	-	-	-
cWC GP + ACGAN (ours)	8.80 ± 0.13	-	17.2	-	-	-
cWC_{sa} GP + ACGAN (ours)	8.69 ± 0.13	-	16.8	-	-	-
SN + Proj. Discr. [16]	8.62	17.5	-	9.04	23.2	-
cWC SN + Proj. Discr. (ours)	8.97 ± .11	16.0	13.5	9.52 ± .07	20.5	17.2
cWC_{sa} SN + Proj. Discr. (ours)	8.85 ± .10	16.5	13.5	9.80 ± .17	20.6	17.4

5.2.1 Ablation study

We analyze all the main aspects of the conditional coloring introduced in Sec. 4 using an SN + ResNet + Proj. Discr. framework for all the baselines presented here. Moreover, in all the baselines, the whitening part is obtained using Eq. (5). We call $cWC-clt-only$ a version of *CondColoring()* with only the class-specific term in Eq. (9). This is implemented simply removing the class-agnostic branch in Fig. 1(b) and learning a specific (Γ_y, β_y) pair per class, without class-filter soft assignment. $cWC_{sa-clt-only}$ is the same as $cWC-clt-only$ but using the soft assignment in Eq. (10). Similarly, we call $cWC-diag$ the baseline in which each Γ_y in Eq. (9) is replaced with a *diagonal* Γ_y matrix. This corresponds to the learn a set of d independent *scalar* parameters for each class y $(\{\gamma_{y,k}, \beta_{y,k}\}_{k=1}^d)$ to represent class-specific information similarly to [11] (see Eq. (8)). In $cWC-diag$ we also use the class-agnostic branch. Note that a class-agnostic branch without any kind of class-specific parameters cannot represent at all class information in the generator. As a reference, in the first row of Tab. 6 we also report the results of exactly the same framework but with our cWC replaced with cBN [11].

The results reported in Tab. 6 show that both the *cls-only* versions are significantly worse than $cWC-diag$ which includes the class-agnostic branch. On the other hand, while on CIFAR-10 $cWC-diag$, cWC and cWC_{sa} reach comparable results, on CIFAR-100 $cWC-diag$ drastically underperforms the other two versions which are based on full coloring matrices. We believe this is because the number of classes (n) in CIFAR-100 is one order of magnitude larger than in CIFAR-10 and, with a large n , the scalar “ γ ” parameters are not sufficient to represent class-specific information. Finally, also the comparison between cWC and cWC_{sa} depends on n , and the advantage of using cWC_{sa} instead of cWC is more evident on the Tiny ImageNet experiment (see Tab.4).

6 Conclusion

In this paper we proposed a whitening and coloring transform which extends both batch normalization [9] and conditional batch normalization [11] taking into account the feature correlations. Our

Table 6: Ablation study of *CondColoring()*.

Method	CIFAR-10		CIFAR-100	
	IS	FID 10k	IS	FID 10K
<i>cBN</i>	7.68 ± .13	22.1	8.08 ± .08	26.5
<i>cWC-cla-only</i>	8.10 ± .09	28.0	7.10 ± .06	75.4
<i>cWC_{sa}-cla-only</i>	8.20 ± .09	23.5	7.88 ± .12	33.4
<i>cWC-diag</i>	8.90 ± .09	14.2	8.82 ± .12	20.8
<i>cWC</i>	8.97 ± .11	13.5	9.52 ± .07	17.2
<i>cWC_{sa}</i>	8.85 ± .10	13.5	9.80 ± .17	17.4

empirical results show that the proposed approach can speed-up the training process and improve the image generation quality of different basic frameworks on different datasets in both the conditional and the unconditional scenario. As a future work, we plan to apply the unconditional WC to discriminative tasks.

Acknowledgements

We want to thank the NVIDIA Corporation for the donation of the GPUs used in this project.

References

- [1] Goodfellow, I.J., Pouget-Abadie, J., Mirza, M., Xu, B., Warde-Farley, D., Ozair, S., Courville, A.C., Bengio, Y.: Generative Adversarial Nets. In: NIPS. (2014) 2672–2680
- [2] Vondrick, C., Pirsiavash, H., Torralba, A.: Generating videos with scene dynamics. In: NIPS. (2016) 613–621
- [3] Gulrajani, I., Ahmed, F., Arjovsky, M., Dumoulin, V., Courville, A.C.: Improved training of Wasserstein GANs. In: NIPS. (2017)
- [4] Odena, A., Olah, C., Shlens, J.: Conditional image synthesis with auxiliary classifier GANs. In: ICML. (2017) 2642–2651
- [5] Isola, P., Zhu, J., Zhou, T., Efros, A.A.: Image-to-image translation with conditional adversarial networks. CVPR (2017)
- [6] Reed, S.E., Akata, Z., Yan, X., Logeswaran, L., Schiele, B., Lee, H.: Generative adversarial text to image synthesis. In: ICML. (2016) 1060–1069
- [7] Ma, L., Jia, X., Sun, Q., Schiele, B., Tuytelaars, T., Gool, L.V.: Pose guided person image generation. In: NIPS. (2017) 405–415
- [8] Siarohin, A., Sangineto, E., Lathuilière, S., Sebe, N.: Deformable GANs for pose-based human image generation. arXiv:1801.00055 (2017)
- [9] Ioffe, S., Szegedy, C.: Batch normalization: Accelerating deep network training by reducing internal covariate shift. In: ICML. (2015)
- [10] Hossain, M.: Whitening and coloring transforms for multivariate gaussian random variables. Project Rhea (2016)
- [11] Dumoulin, V., Shlens, J., Kudlur, M.: A learned representation for artistic style. arXiv:1610.07629 (2016)
- [12] Ba, L.J., Kiros, R., Hinton, G.E.: Layer normalization. arXiv:1607.06450 (2016)
- [13] Luo, P.: Learning deep architectures via generalized whitened neural networks. In: ICML. (2017)
- [14] Mirza, M., Osindero, S.: Conditional generative adversarial nets. arXiv:1411.1784 (2014)
- [15] Perarnau, G., van de Weijer, J., Raducanu, B., Álvarez, J.M.: Invertible conditional GANs for image editing. arXiv:1611.06355 (2016)

- [16] Miyato, T., Koyama, M.: cGANs with projection discriminator. In: ICLR. (2018)
- [17] Ulyanov, D., Vedaldi, A., Lempitsky, V.S.: Instance normalization: The missing ingredient for fast stylization. arXiv:1607.08022 (2016)
- [18] Schäfer, J., Strimmer, K.: A shrinkage approach to large-scale covariance matrix estimation and implications for functional genomics. *Statistical Applications in Genetics and Molecular Biology* **4**(1) (2005)
- [19] Dereniowski, D., Marek, K.: Cholesky factorization of matrices in parallel and ranking of graphs. In: 5th Int. Conference on Parallel Processing and Applied Mathematics. (2004)
- [20] Abadi, M., Agarwal, A., Barham, P., Brevdo, E., Chen, Z., Citro, C., Corrado, G.S., Davis, A., Dean, J., Devin, M., Ghemawat, S., Goodfellow, I., Harp, A., Irving, G., Isard, M., Jia, Y., Jozefowicz, R., Kaiser, L., Kudlur, M., Levenberg, J., Mané, D., Monga, R., Moore, S., Murray, D., Olah, C., Schuster, M., Shlens, J., Steiner, B., Sutskever, I., Talwar, K., Tucker, P., Vanhoucke, V., Vasudevan, V., Viégas, F., Vinyals, O., Warden, P., Wattenberg, M., Wicke, M., Yu, Y., Zheng, X.: TensorFlow: Large-scale machine learning on heterogeneous systems (2015) Software available from tensorflow.org.
- [21] : Optimal whitening and decorrelation. *The American Statistician* (2018)
- [22] He, K., Zhang, X., Ren, S., Sun, J.: Deep residual learning for image recognition. In: CVPR. (2016) 770–778
- [23] Torralba, A., Fergus, R., Freeman, W.T.: 80 million tiny images: A large data set for nonparametric object and scene recognition. *IEEE Trans. Pattern Anal. Mach. Intell.* **30**(11) (2008) 1958–1970
- [24] Coates, A., Ng, A.Y., Lee, H.: An analysis of single-layer networks in unsupervised feature learning. In: AISTATS. (2011)
- [25] Salimans, T., Goodfellow, I.J., Zaremba, W., Cheung, V., Radford, A., Chen, X.: Improved techniques for training GANs. In: NIPS. (2016) 2226–2234
- [26] Heusel, M., Ramsauer, H., Unterthiner, T., Nessler, B., Hochreiter, S.: GANs trained by a two time-scale update rule converge to a local nash equilibrium. In: NIPS. (2017)
- [27] LeCun, Y., Bottou, L., Bengio, Y., Haffner, P.: Gradient-based learning applied to document recognition. *Proceedings of the IEEE* **86**(11) (1998) 2278–2324
- [28] Xiao, H., Rasul, K., Vollgraf, R.: Fashion-mnist: a novel image dataset for benchmarking machine learning algorithms. arXiv:1708.07747 (2017)
- [29] Miyato, T., Kataoka, T., Koyama, M., Yoshida, Y.: Spectral normalization for generative adversarial networks. arXiv:1802.05957 (2018)
- [30] Radford, A., Metz, L., Chintala, S.: Unsupervised representation learning with deep convolutional generative adversarial networks. ICLR (2015)
- [31] Karras, T., Aila, T., Laine, S., Lehtinen, J.: Progressive growing of GANs for improved quality, stability, and variation. In: ICLR. (2018)
- [32] Dumoulin, V., Belghazi, I., Poole, B., Lamb, A., Arjovsky, M., Mastropietro, O., Courville, A.C.: Adversarially learned inference. arXiv:1606.00704 (2016)
- [33] Berthelot, D., Schumm, T., Metz, L.: BEGAN: boundary equilibrium generative adversarial networks. arXiv:1703.10717 (2017)
- [34] Dai, Z., Almahairi, A., Bachman, P., Hovy, E.H., Courville, A.C.: Calibrating energy-based generative adversarial networks. arXiv:1702.01691 (2017)
- [35] Warde-Farley, D., Bengio, Y.: Improving generative adversarial networks with denoising feature matching. (2017)

- [36] Wei, X., Liu, Z., Wang, L., Gong, B.: Improving the improved training of wasserstein GANs. In: ICLR. (2018)
- [37] Salimans, T., Zhang, H., Radford, A., Metaxas, D.: Improving GANs using optimal transport. In: ICLR. (2018)
- [38] Wang, D., Liu, Q.: Learning to draw samples: With application to amortized MLE for generative adversarial learning. arXiv:1611.01722 (2016)
- [39] Huang, X., Li, Y., Poursaeed, O., Hopcroft, J.E., Belongie, S.J.: Stacked generative adversarial networks. In: CVPR. (2017)
- [40] Zhou, Z., Cai, H., Rong, S., Song, Y., Ren, K., Zhang, W., Wang, J., Yu, Y.: Activation maximization generative adversarial nets. In: ICLR. (2018)
- [41] Giles, M.: An extended collection of matrix derivative results for forward and reverse mode automatic differentiation. (2008)
- [42] Walter, S.: Structured higher-order algorithmic differentiation in the forward and reverse mode with application in optimum experimental design. (2012) 82–84

A Implementation details

In our experiments we use 2 basic network architectures: ResNet [3] and DCGAN [29]. For a fair comparison, we strictly follow the training protocol details reported in [3, 29] and provided in the two subsections below. Moreover, we adopt the same architectural details suggested in [3, 29] (e.g., the number of blocks, the number of 3×3 convolutional filters, etc.), except the use of our WC/cWC layers in our generators. The only difference with respect to the architectural setup in [3, 29] is emphasized in the appendix A.2 and concerns a different ratio between the number of 3×3 convolutional filters in the generator versus the number of discriminator’s convolutional filters.

A.1 Unconditional image generation experiments

In all our *GP*-based experiments we use Adam with learning rate $\alpha = 2e-4$, first momentum $\beta_1 = 0$ and second momentum $\beta_2 = 0.9$. The learning rate is linearly decreased till it reaches 0. In all the *GP*-based experiments we use the WGAN loss + Gradient Penalty [3], while in the *SN*-based experiment we use the hinge loss [29]. In all the *GP* experiments we train the networks for 100k iterations following [3]. In the CIFAR-10 experiment, *SN + ResNet* was trained for 50k iterations [29]. In the STL-10 experiment, we train the networks for 100k iterations following [29]. Each iteration is composed of 1 generator update with batch size 128 and 5 discriminator updates with batch size $64 + 64$ (i.e., 64 generated and 64 real images), same numbers are used in [3, 29]. When training the DCGAN architectures we use two times more iterations. However, in DCGAN each iteration is composed of 1 generator update with batch size 64 and 1 discriminator update with batch size $64 + 64$ [29]. In all the experiments we use the original image resolution, except for STL-10 where we downsample all images to 48×48 following Miyato et al. [16].

We provide below the architectural details of our networks. We denote with C_d^S a block consisting of the following layer sequence: (1) either a WC or a cWC layer (depending on the unconditional/conditional scenario, respectively), (2) a ReLU and (3) a convolutional layer with d output filters. The output of this block has the *same* (S) spatial resolution of the input. C_d^D is similar to C_d^S , but the output feature map is *downsampled* (D): the convolutional layer uses *stride* = 2. C_d^U is an *upconvolution* (U) block with fractional *stride* = 0.5. We use a similar notation for the ResNet blocks: R_d^S is a ResNet block (see Fig.1(a)) which preserves spatial resolution. R_d^D downsamples the feature maps and R_d^U upsamples the feature maps. Also we denote with: (1) D_k a dense layer with k outputs, (2) G a global-sum-pooling layer, (3) F a flattening layer, (4) P_h a layer that permutes the dimensions of the input feature map to the target spatial resolution $h \times h$. Given the above definitions, we show in Tab. 7 the architectures used for the unconditional image generation experiments. We again emphasize that the methods we compare with in Tab. 2 (left) have the same network structure except the use of WC layers in the generator.

A.2 Conditional image generation experiments

In the conditional image generation experiments, most of the hyper-parameter values are the same as in the appendix A.1. In the CIFAR-10 experiment with *GP + ACGAN*, we train the networks for 100k iterations following [3]. In the CIFAR-10 and CIFAR-100 experiments with *SN* and *Projection Discriminator* we train the networks for 50k iterations following [16]. In the Tiny ImageNet experiments, we train the networks for 100k iterations. All the other hyper-parameters are the same as in the appendix A.1.

Tab. 8 shows the architectures used in the conditional image generation experiments.

Both *cWC SN + Proj. Discr.* and *cWC_{sa} SN + Proj. Discr.* used in CIFAR-10 and CIFAR-100 (see Tab. 5) have an opposite generator/discriminator filter number ratio with respect to the ratio used in *SN + Proj. Discr.* [16]. In fact, we decrease the number of 3×3 convolutional filters in each generator block from 256, used in [16], to 128. Simultaneously, we increase the number of 3×3 convolutional filters in the discriminator from 128 [16] to 256. *This is the only difference between our cWC-based frameworks and [16] in the experiments of Tab. 5 in the main paper.* The reason behind this architectural choice is that we hypothesize our cWC generators are more powerful than the corresponding discriminators. Using the same generator/discriminator filter ratio as in [16], we perform on par with *SN + Proj. Discr.* [16]. In Tab. 6 of main paper, *cBN* refers to *SN + Proj. Discr.* with the 128/256 filter ratio above mentioned and used in the cWC baselines.

In Fig. 3 we show a schematic representation of the baselines reported in Tab. 6 of the main paper.

Finally, in Tab. 2 (right) and in Tab. 5, *cWC SN + Proj. Discr.* indicates exactly the same framework, the only difference being a different learning rate policy. The results of *cWC SN + Proj. Discr.* reported in Tab. 5 have been obtained using the same learning rate policy as in [16]. However, our model already achieved its peak performance after 30k iterations. Hence, we decreased the learning rate by a factor of 10 at iteration 30k and then we trained *cWC SN + Proj. Discr.* for additional 1k iterations. This brought to a performance boost, as reported in Tab. 2 (right).

A.3 Evaluation

In our experiments we use 2 evaluation measures: Inception Score (IS) [25] and the Fréchet Inception Distance (FID) [26].

IS was originally introduced by Salimans et al. [25]. The authors in [25] suggest to measure IS using 5k generated images, repeat this generation 10 times and then average the results. We follow exactly the same protocol.

FID is a more recent metric and the evaluation protocol is less consolidated. Miyato et al. [16] suggest to compute FID using 10k images from the test set together with 5k generated images. Heusel et al. [26] suggest to use a sample sizes of at least 10k real and 10k generated images. In the main paper, FID 5k refers to the former protocol [16] and FID 10k refers to the second protocol [26].

Table 7: The architectures used in the unconditional image generation experiments. All the generators have a *tanh* nonlinearity at the end. We use WC in all the blocks of the generators.

Method	Generator	Discriminator
CIFAR-10		
WC GP + ResNet	$D_{2048} - P_4 - R_{128}^U - R_{128}^U - R_{128}^U - C_3^S$	$R_{128}^D - R_{128}^D - R_{128}^S - R_{128}^S - G - D_1$
WC SN + DCGAN	$D_{8192} - P_4 - C_{512}^U - C_{256}^U - C_{128}^U - C_3^S$	$C_{64}^S - C_{128}^D - C_{128}^S - C_{256}^D - C_{256}^S - C_{512}^D - C_{512}^S - F - D_1$
WC SN + ResNet	$D_{4096} - P_4 - R_{256}^U - R_{256}^U - R_{256}^U - C_3^S$	$R_{128}^D - R_{128}^D - R_{128}^S - R_{128}^S - G - D_1$
STL-10		
WC SN + DCGAN	$D_{18432} - P_6 - C_{512}^U - C_{256}^U - C_{128}^U - C_3^S$	$C_{64}^S - C_{128}^D - C_{128}^S - C_{256}^D - C_{256}^S - C_{512}^D - C_{512}^S - F - D_1$
WC SN + ResNet	$D_{9216} - P_6 - R_{256}^U - R_{256}^U - R_{256}^U - C_3^S$	$R_{128}^D - R_{128}^D - R_{128}^S - R_{128}^S - G - D_1$

Table 8: The architectures used in the conditional image generation experiments. All the generators have a *tanh* nonlinearity at the end. We use cWC in all the blocks of the generators, except for the last C_3^S block in which we use WC.

Method	Generator	Discriminator
CIFAR-10 and CIFAR-100		
cWC GP + ACGAN	$D_{2048} - P_4 - R_{128}^U - R_{128}^U - R_{128}^U - C_3^S$	$R_{128}^D - R_{128}^D - R_{128}^S - R_{128}^S - G - D_1$
cWC SN + Proj. Discr.	$D_{2048} - P_4 - R_{128}^U - R_{128}^U - R_{128}^U - C_3^S$	$R_{256}^D - R_{256}^D - R_{256}^S - R_{256}^S - G - D_1$
Tiny ImageNet		
cWC SN + Proj. Discr.	$D_{2048} - P_4 - R_{128}^U - R_{128}^U - R_{128}^U - R_{128}^U - C_3^S$	$R_{64}^D - R_{128}^D - R_{256}^S - R_{512}^D - R_{1024}^S - G - D_1$

B Experiments using small-size datasets

In this section we show additional experiments using two small-size datasets: the MNIST [27] and the Fashion-MNIST dataset [28] (see Fig. 7 for some generated image examples). In both cases we use the *SN + ResNet* architecture described in Tab. 9. On MNIST we train for 5k iterations with a constant learning rate, while on Fashion-MNIST we train for 20k iterations with a linearly decaying learning rate (see the appendix A.1). All the other hyper-parameters are the same as in the appendix A.1.

The results are reported in Tab. 10. MNIST (unconditional scenario) is the only dataset where we did not observe an improvement using our WC. However, on the more challenging Fashion-MNIST dataset, we did observe an improvement, especially in the conditional scenario.

Table 9: The MNIST and the Fashion-MNIST architectures. All the generators have a *tanh* nonlinearity at the end. In the unconditional scenario we use WC in all the blocks of the generators. In the conditional scenario, we use cWC in all the blocks of the generators but the last C_3^S block in which we use WC.

Method	Generator	Discriminator
WC	$D_{12544} - P_7 - R_{256}^U - R_{256}^U - C_3^S$	$R_{128}^D - R_{128}^D - R_{128}^S - R_{128}^S - G - D_1$
cWC	$D_{6272} - P_7 - R_{128}^U - R_{128}^U - C_3^S$	$R_{128}^D - R_{128}^D - R_{128}^S - R_{128}^S - G - D_1$

Table 10: FID 10k scores for the unconditional and the conditional scenarios on MNIST and Fashion-MNIST.

Method	MNIST	Fashion-MNIST
Unconditional		
BN	3.6	10.6
WC	4.9	10.4
Conditional		
cBN	4.5	7.5
cWC	4.3	6.2

C Back-propagation

In our implementation, the gradient back-propagation through our WC/cWC layers is obtained by relying on the TensorFlow [20] automatic differentiation. However, for completeness and to make our method fully-reproducible, in this section we provide a *reverse mode automatic differentiation* (AD) [41, 9, 42] of the Whitening back-propagation steps. Note that, since (conditional and unconditional) Coloring is implemented using convolution operations, back-propagation for Coloring is straightforward.

In the following we adopt Giles' notation [41] that we shortly present below. Given a scalar function of a matrix $f(A)$, \bar{A} indicates the reverse mode AD sensitivities with respect to A , i.e.: $\bar{A} = \frac{\partial f(A)}{\partial A}$.

Given a batch B , we subtract the mean μ_B from each sample $\mathbf{x}_i \in B$. Reverse mode AD mean-subtraction is trivial and described in Ioffe et al. [9]. We then stack all the mean-subtracted samples in a matrix $X \in \mathbb{R}^{d \times m}$ (where we drop the B subscript for simplicity). Using this notation, the covariance matrix Σ (Eq.(6)) is given by: $\Sigma = \frac{1}{m-1} X X^T$.

In the Cholesky decomposition we have: $\Sigma = L^T L$, $W = L^{-1}$. We can rewrite Eq. (3) as a matrix multiplication and obtain $Y = W X$, where i -th column of Y is $\hat{\mathbf{x}}_i$.

In reverse mode AD, \bar{Y} is given and we need to compute \bar{X} . Using the formulas in [41] we obtain:

$$\bar{W} = \bar{Y} X^T, \quad (11)$$

$$\bar{L} = -W^T \bar{W} W^T \quad (12)$$

Now, using the formulas in [42]:

$$\bar{\Sigma} = \frac{1}{2} L^{-T} (P \circ L^T \bar{L} + (P \circ L^T \bar{L})^T) L^{-1} = -\frac{1}{2} W^T (P \circ \bar{W} W^T + (P \circ \bar{W} W^T)^T) W \quad (13)$$

where:

$$P = \begin{pmatrix} \frac{1}{2} & 0 & \cdots & 0 \\ 1 & \frac{1}{2} & \ddots & 0 \\ 1 & \ddots & \ddots & 0 \\ 1 & \cdots & 1 & \frac{1}{2} \end{pmatrix}$$

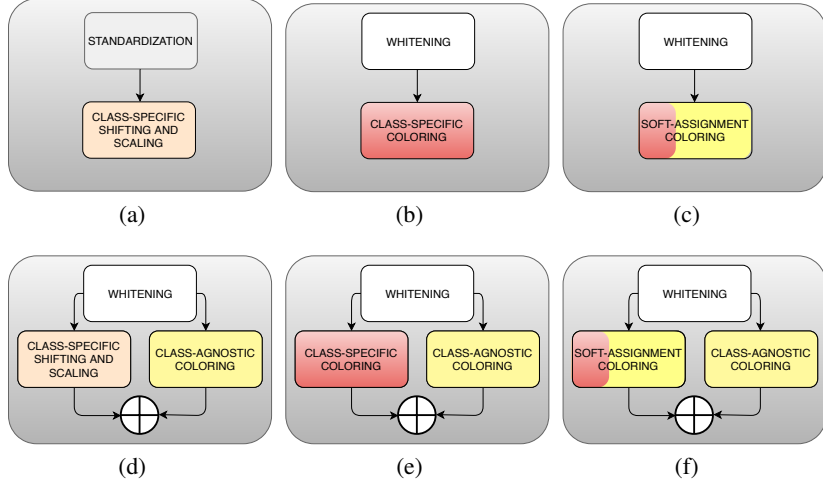


Figure 3: A schematic representation of the baselines used in Tab. 6 of the main paper: (a) *cBN* conditional batch normalization; (b) *cWC-clt-only* coloring with only the conditional branch; (c) *cWCsa-clt-only* coloring with only the conditional branch based on the class-filter soft assignment; (d) *cWCdiag* with 2 branches and a diagonal matrix Γ_y ; (e) *cWC* plain version; (f) *cWCsa* version with soft assignment.

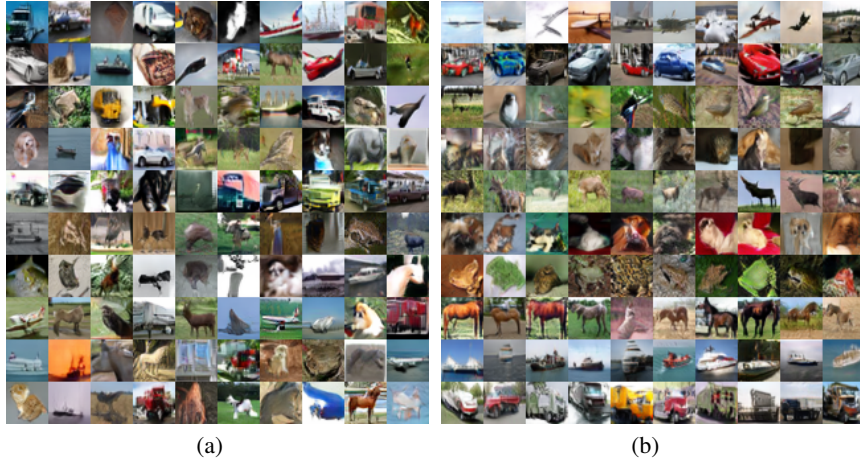


Figure 4: CIFAR-10 images generated using: (a) *WC SN + ResNet* and (b) *cWC SN + ResNet* (samples of the same class displayed in the same row).

and \circ is Hadamard product.

Referring again to [41], and combining the reverse sensitives with respect to X from the 2 streams we get:

$$\bar{X} = \frac{2}{m-1} \bar{\Sigma} X + W^T \bar{Y} \quad (14)$$

D Qualitative results

In this section we show some qualitative results obtained using our WC/cWC methods. Specifically, examples of images generated using the CIFAR-10 dataset are shown in Fig. 4. Fig. 5 (a)-Fig. 5 (b) show examples generated on the STL-10 and the CIFAR-100 dataset, respectively. In Fig. 6 we show Tiny ImageNet samples. Finally, Fig. 7 shows MNIST and Fashion-MNIST generated images.

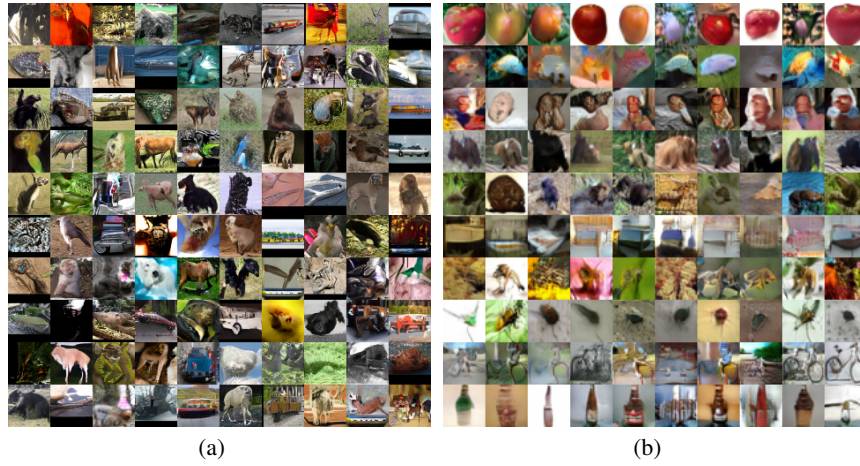
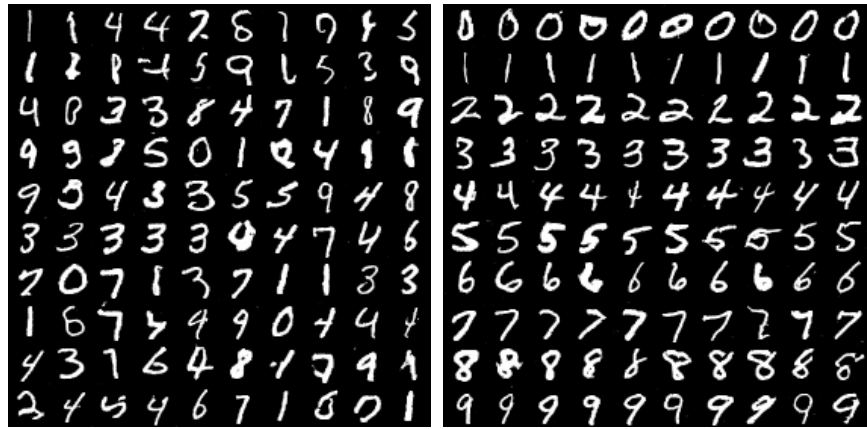


Figure 5: Qualitative results: (a) STL-10 images generated using WC and (b) CIFAR-100 images generated using cWC_{sa} (first 10 CIFAR-100 classes, samples of the same class are displayed in the same row).

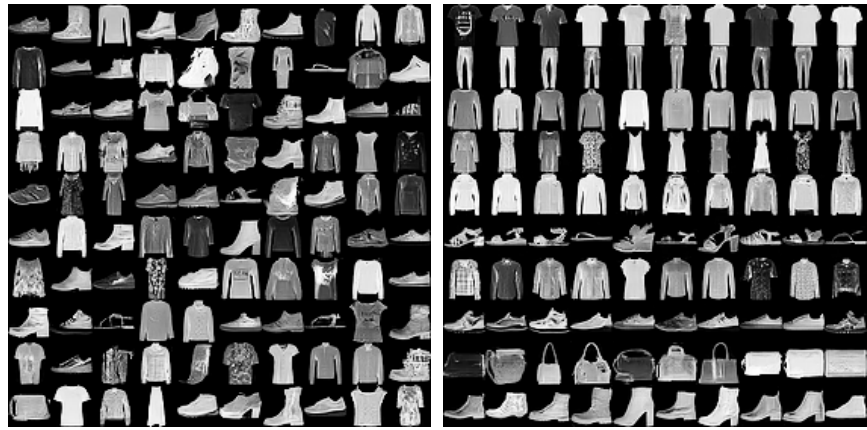


Figure 6: Tiny ImageNet images generated using cWC_{sa} by randomly selecting 10 classes (samples of the same class are displayed in the same row).



(a)

(b)



(c)

(d)

Figure 7: MNIST (a, b) and Fashion-MNIST (c, d) images generated using WC (a, c) and cWC (b, d).